Angewandte Chemie
Eine Zeitschrift der Gesellschaft Deutscher Chemiker

Supporting Information

Electronic Regulation of Nickel Single Atoms by Confined Nickel Nanoparticles for Energy-Efficient CO_2 Electroreduction

W. Ren, X. Tan, C. Jia, A. Krammer, Q. Sun, J. Qu, S. C. Smith, A. Schueler, X. Hu, C. Zhao**

Methods

Synthesis of NiSA/NP catalyst. 0.3 g of $Ni(NO_3)_2 \cdot 6H_2O$ and 3 g of melamine were manually ground for 10 min to get the uniform light-green solid precursor. It was then annealing in the tube furnace in Ar atmosphere at 1000 °C for 2h with a heating rate of 5 °C min^{-1}. The final NiSA/NP catalyst can be obtained by washing the sintered powder with 3 M HCl for 5 h to remove the impurities and Ni nanoparticles outside of CNTs.

Synthesis of NiSA catalyst. The NiSA catalyst was prepared by the NH_4Cl treatment method. Namely, 0.1 g of NiSA/NP and 3 g of NH_4Cl were manually ground for 10 min to get the uniform black precursor. It was then annealing in the tube furnace in Ar atmosphere at 1000 °C for 2 h with a heating rate of 5 °C min^{-1}. The final NiSA catalyst can be obtained by washing the sintered powder with 3 M HCl for 5 h to remove the impurities outside of CNTs. The NiSA, NiSA-2, and NiSA-3 represent the NH_4Cl treatments for 1, 2 and 3 times, respectively.

Synthesis of NiNP catalyst. The pure carbon-encapsulated NiNP catalyst without Ni-N-C sites was prepared by using nitrogen-free precursors. Namely, 2 g of fumaric acid, 1 g of nickel acetate, and 3 g of sodium carbonate were manually ground for 10 min to get the uniform light-green solid precursor. It was then annealed in the tube furnace in Ar atmosphere at 700 °C for 1 h with a heating rate of 5 °C min^{-1}. The final NiNP catalyst can be obtained by washing the sintered powder with 3 M HCl for 5 h to remove the impurities and Ni nanoparticles outside of CNTs.

Characterizations. Scanning electron microscope (SEM) images were collected with a QUANTA 450. Transmission electron microscopy (TEM), high-resolution TEM (HRTEM), high angle annular dark-field scanning TEM (HAADF-STEM) were carried out on JEOL JEM-ARM200f microscope at 200 kV. XRD was performed on a PANalytical X'Pert X-ray diffraction system (45 kV, 40 mA, Cu Kα radiation). XPS results were recorded by Thermo ESCALAB250Xi. XAFS spectra at the Ni K-edge were collected in the Australia Synchrotron center in fluorescence mode. UPS was performed on a SPECS Leybold EA11 MCD electron spectrometer and the base pressure in the measurement chamber is in the range of $5*10^{-10}$ mbar. The spectrometer is equipped with a He discharge lamp for UPS (He II at $h\nu = 40.82$ eV). EPR spectra were conducted on a benchtop spectrometer Bruker EMXnano with *x* band.

Electrochemical measurements. CO_2 electrolysis in H-cells was performed in a gas-tight H-cell with two compartments separated by a cation exchange membrane (Nafion®117). A Pt plate was used as the counter electrode, a saturated calomel electrode (SCE) was used as the

reference electrode, and CO_2-saturated 0.5 M $KHCO_3$ was used as the electrolyte, respectively. To prepare the working electrodes, 10 mg of catalyst and 100 μL of 5% Nafion solution were introduced into 100 μL of water and 300 μL of ethanol solution and sonicated for 1 h. A 6.25 μL of the catalyst ink was coated onto a carbon fiber paper substrate and dried in the air, giving an effective area of 0.25 cm^2 with catalyst loading of 0.5 mg cm^{-2}. With the same catalysts loading, the content of Ni single-atom in NiSA electrodes could be slighter higher than in NiSA/NP electrodes due to the removal of Ni nanoparticles. In H-cells, LSV and potentiostatic data were corrected with an *iR* compensation.

CO_2 electrolysis in flow cells. The windows for electrolysis were set to 1 cm × 1 cm. Each chamber has an inlet and an outlet for electrolyte, and an Ag/AgCl reference electrode was placed in the catholyte chamber. The catalyst ink was prepared by mixing 10 mg of catalyst, 3 mL of ethanol and 100 μL of a Nafion perfluorinated resin solution. Then, catalysts were air-brushed onto 3 × 3 cm^2 38 BC gas diffusion layer (FuelCellStore) electrodes and cut into 4 pieces of 1.5 × 1.5 cm^2 electrodes for electrochemical testing. Commercial IrO_2 sprayed on Titanium mesh was used as a counter electrode for oxygen evolution reaction (OER). An anion exchange membrane (FAA-3-50, FuelCellStore) was used to separate the cathode and anode chambers. 1 M KOH solution was used as the electrolytes. The catholyte and anolyte were cycled at a flow rate of 10 mL min^{-1} by using a peristaltic pump. LSV and potentiostatic data were corrected with an *iR* compensation.

CO_2 electrolysis in zero-gap MEA device. The windows for electrolysis were set to 1 cm^2. Cathode and anode chambers have an inlet and an outlet for gas and electrolyte, respectively. Both the cathode and anode catalyst ink were prepared by mixing 10 mg of catalyst, 3 mL of ethanol and 100 μL of a Nafion perfluorinated resin solution. Then, the cathode catalyst was air-brushed onto 3 × 3 cm^2 38 BC gas diffusion layer (FuelCellStore) electrodes, and the anode catalyst was air-brushed onto 3 × 3 cm^2 35 AA carbon paper (Ion Power) electrodes. An Sustainion® X37-50 was used as the membrane. The cathode was feed with humidified CO_2 gas and the anode was feed with 1 M KOH electrolytes. The applied cell voltages were recorded without *iR* compensation.

DFT calculations. All of the spin-polarized DFT calculations were performed using the VASP program,[1-3] which uses a plane-wave basis set and a projector augmented wave method (PAW) for the treatment of core electrons. The Perdew, Burke, and Ernzerhof exchange-correlation functional within a generalized gradient approximation (GGA-PBE)[4] was used in our

calculations, and the van der Waals (vdW) correction proposed by Grimme (DFT-D3)[5] was employed due to its good description of long-range vdW interactions. For the expansion of wavefunctions over the plane-wave basis set, a converged cutoff was set to 450 eV.

DFT model 1: Ni-nitrogen-doped carbon catalysts (bare NiN_3) were modelled by (5 × 4) graphene supercells with periodical boundary conditions (Figure S13a). In order to simulate NiN_3@Ni(111) systems, we put Ni-nitrogen-doped carbon on the top of Ni(111) surface. Here, we considered NiN_3 moiety surrounded by Ni(111). A vacuum of 12 Å along the *z*-direction was used. The Brillouin zone was sampled using (2 × 4 × 1) Monkhorst–Pack k-point mesh. In geometry optimizations, all the atomic coordinates were fully relaxed up to the residual atomic forces smaller than 0.01 eV/Å, and the total energy was converged to 10^{-4} eV. The electron distribution and transfer mechanism were determined by using Bader analysis.[6]

DFT model 2: Graphene/Ni(111) systems were modelled by four layers of Ni(111) and one layer of graphene in (5 × 5) supercell with periodical boundary conditions, as shown in Figure S14. During structure optimizations, the graphene monolayers and top two layers of the Ni were allowed to move. In order to simulate the Ni-nitrogen-doped carbon catalysts, a (5 × 5) graphene supercell with periodical boundary conditions was used, and then, some carbon atoms were removed to create NiN_3. A vacuum of 12 Å along the *z*-direction was used. The Brillouin zone was sampled using (3 × 3 × 1) Γ-centred mesh. In geometry optimizations, all the atomic coordinates were fully relaxed up to the residual atomic forces smaller than 0.01 eV/Å, and the total energy was converged to 10^{-4} eV. The electron distribution and transfer mechanism were determined by using Bader analysis.[6]

For CO_2RR on Ni-nitrogen-doped carbon catalysts, we considered the reaction mechanism of CO_2RR to CO through the adsorbed intermediates $COOH^*$ and CO^*. The free energy changes at each electrochemical step involving a proton-electron transfer were computed based on the computational hydrogen electrode (CHE) model,[7] in which the free energy of $(H^+ + e^-)$ equals to $\frac{1}{2}H_2(g)$ for standard hydrogen electrode (SHE). The free energy of adsorbates and non-adsorbed gas-phase molecules is calculated as $G = E_{elec} + E_{ZPE} + \int C_P dT - TS$, where E_{elec} is the electronic energy calculated by DFT; E_{ZPE} is the zero point energy (ZPE), C_P is heat capacity, T is temperature and S is entropy. Here, the correction terms are present in Table S1, which are from previous literature.[8] Additionally, a correction of -0.51 eV for non-adsorbed gas-phase CO molecule has to be made due to the use of PBE functional.[7] The solvation effects have been included for COOH* and CO* by stabilizing 0.25 and 0.10 eV, respectively.[7-9]

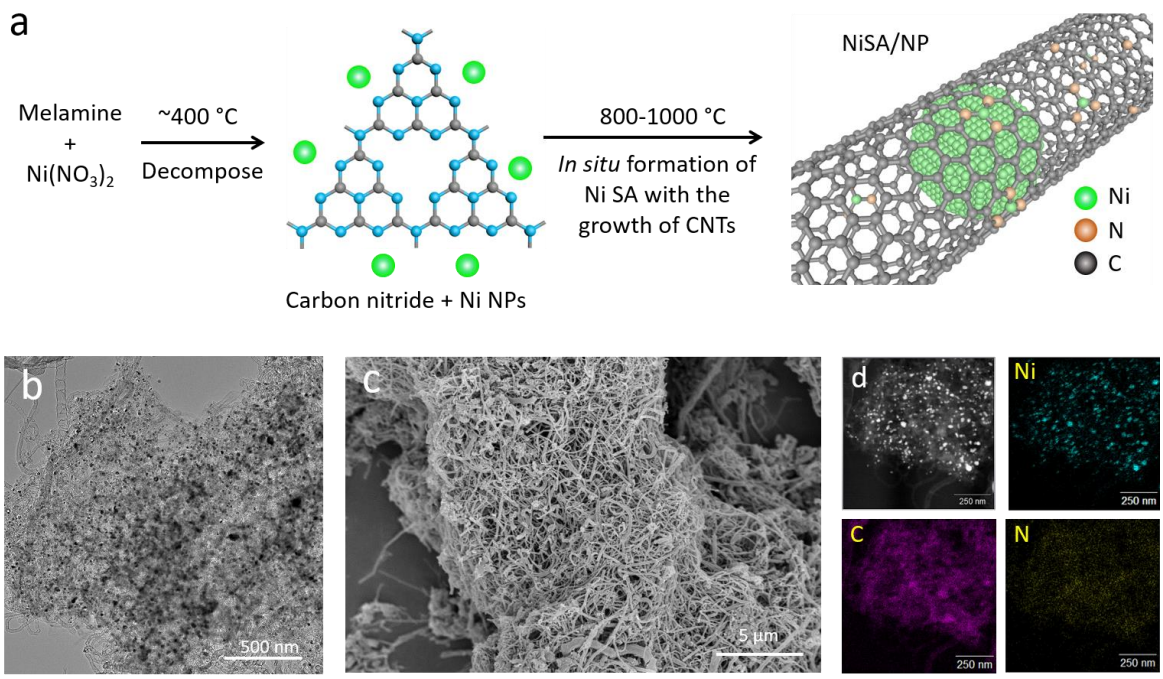

Supplementary Figure 1 | Synthesis and characterization of NiSA/NP. (**a**) The schematic illustration of the formation mechanism of Ni single atom on nanoparticle catalyst. (**b**) TEM, (**c**) SEM, and (**d**) EDS mapping of NiSA/NP.

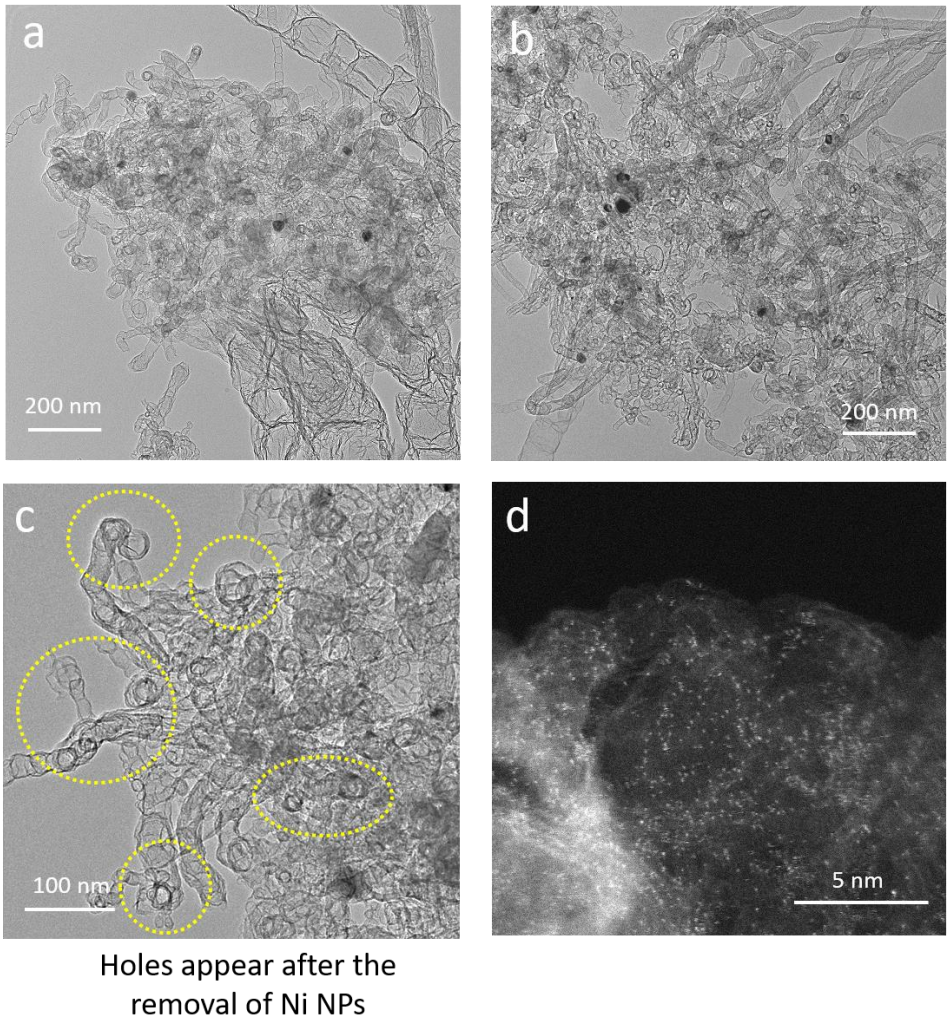

Supplementary Figure 2 | TEM images of NiSA. (**a-c**) TEM and (**d**) HAADF-STEM images of NiSA. Most of the Ni NPs in NiSA/NP were removed after the NH_4Cl treatment and the holes inside of CNTs formed.

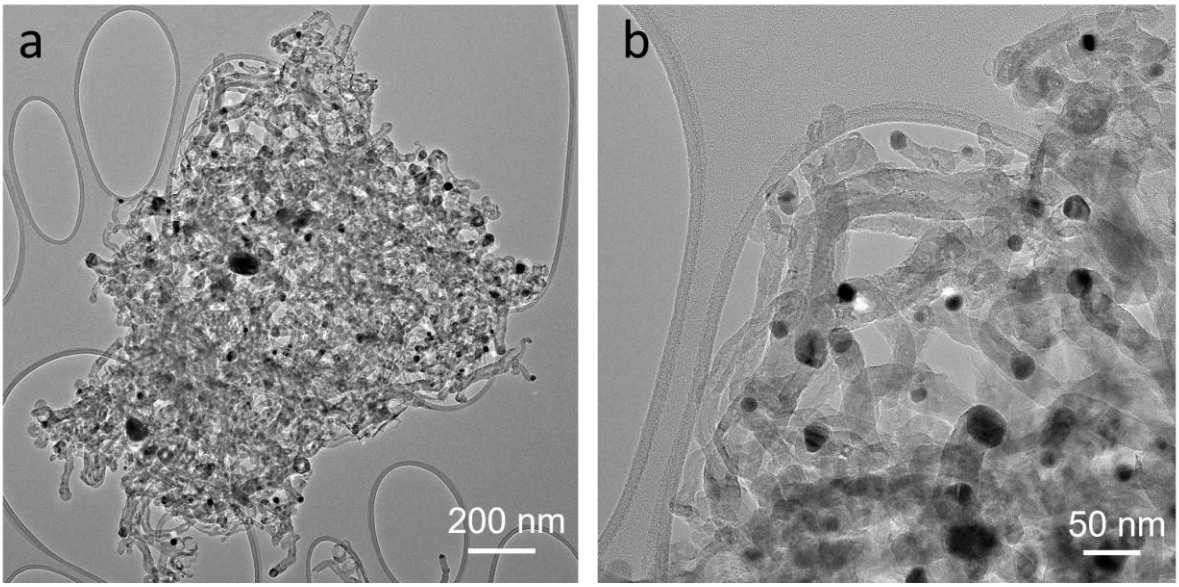

Supplementary Figure 3 | TEM images of pure carbon-encapsulated NiNP catalyst without Ni-N-C sites.

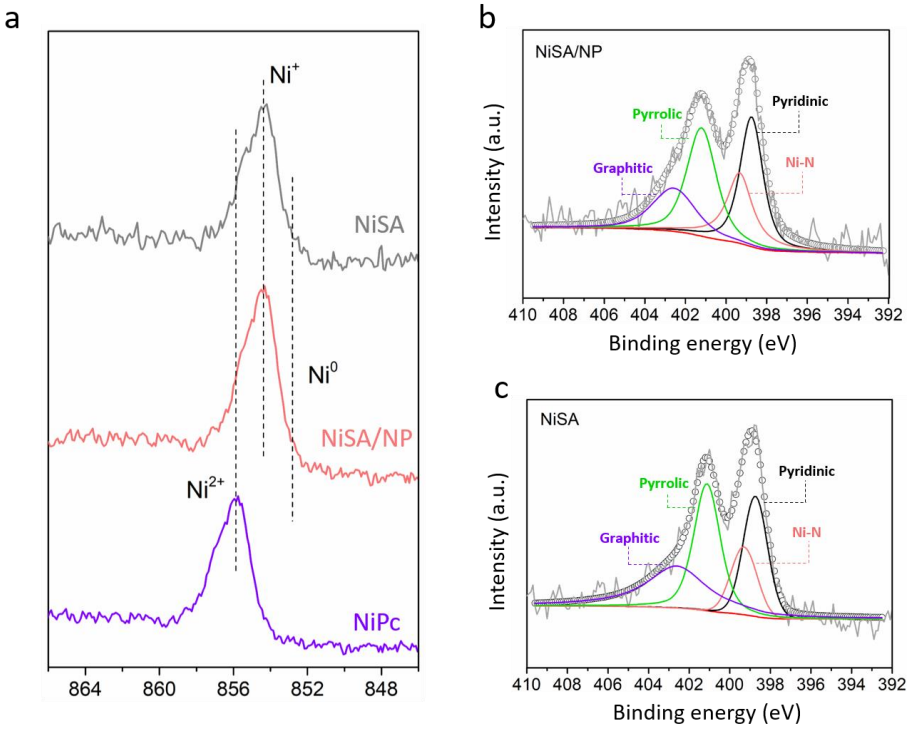

Supplementary Figure 4 | X-ray photoelectron spectroscopy (XPS) analysis. (**a**) Ni 2p spectra of NiSA, NiSA/NP and NiPc. N 1s spectra of NiSA/NP (**b**), and NiSA (**c**).

According to the DFT calculation, the valence of Ni single atom in NiN_3 decreases from +0.78 to +0.7 after electronic donation (Fig. S14d). The change of 0.08 in valence state is not distinguishable in Ni 2p XPS analysis as shown in Figure S4a. Besides, no metallic Ni peak can be observed in XPS, which can be attributed to the fully confined Ni nanoparticles inside of CNTs that exceed the detection limit of XPS.

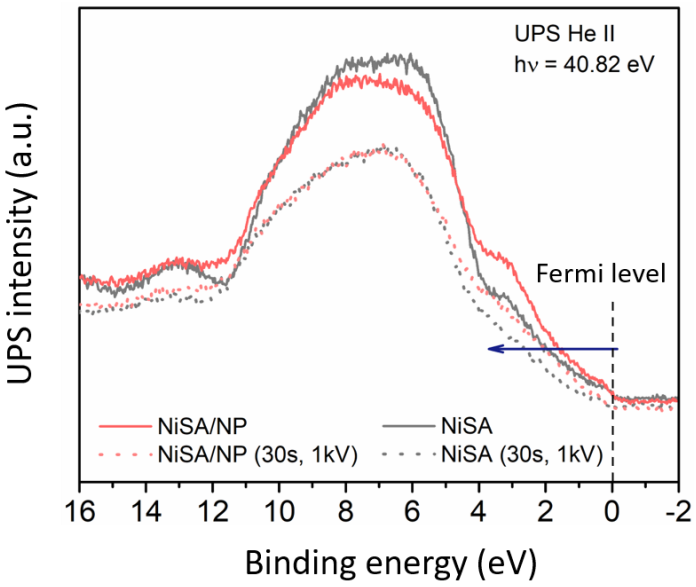

Supplementary Figure 5 | Normalized UPS He II spectra of NiSA/NP and NiSA before and after an Ar sputter cleaning of 30 s at 1 kv.

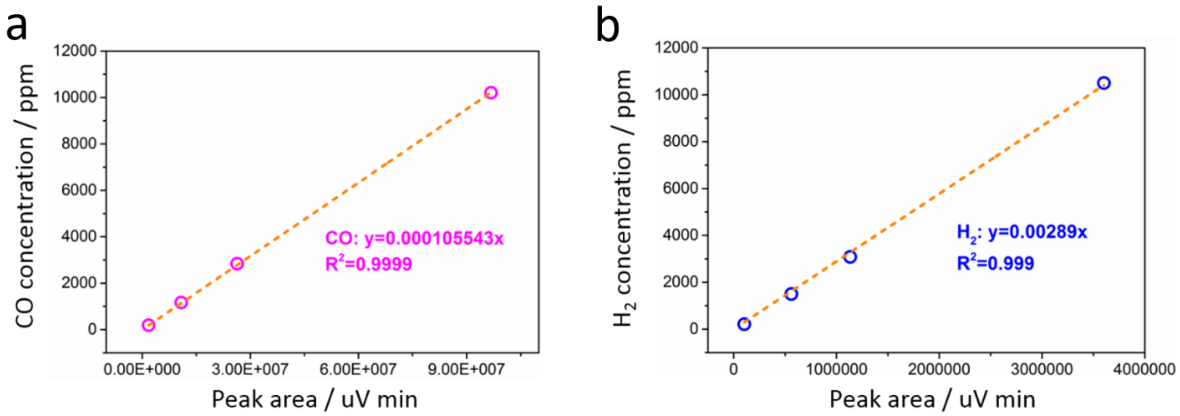

Supplementary Figure 6 | GC Calibration curves for (a) CO and (b) H_2 quantification.

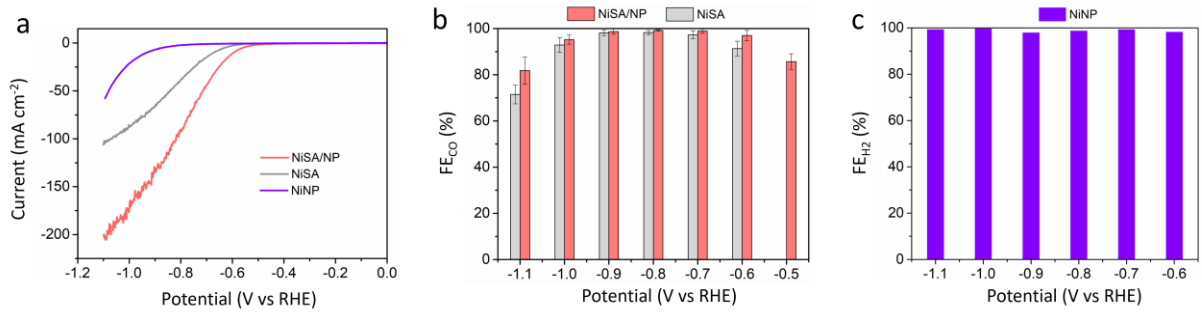

Supplementary Figure 7 | CO_2RR in H-cells. (**a**) LSV curves of NiSA/NP, NiSA, and NiNP in CO_2 atmosphere. (**b**) FE_{CO} of NiSA/NP and NiSA from -0.5 V to -1.1 V vs RHE. (**c**) FE_{H2} of NiNP from -0.6 V to -1.1 V vs RHE.

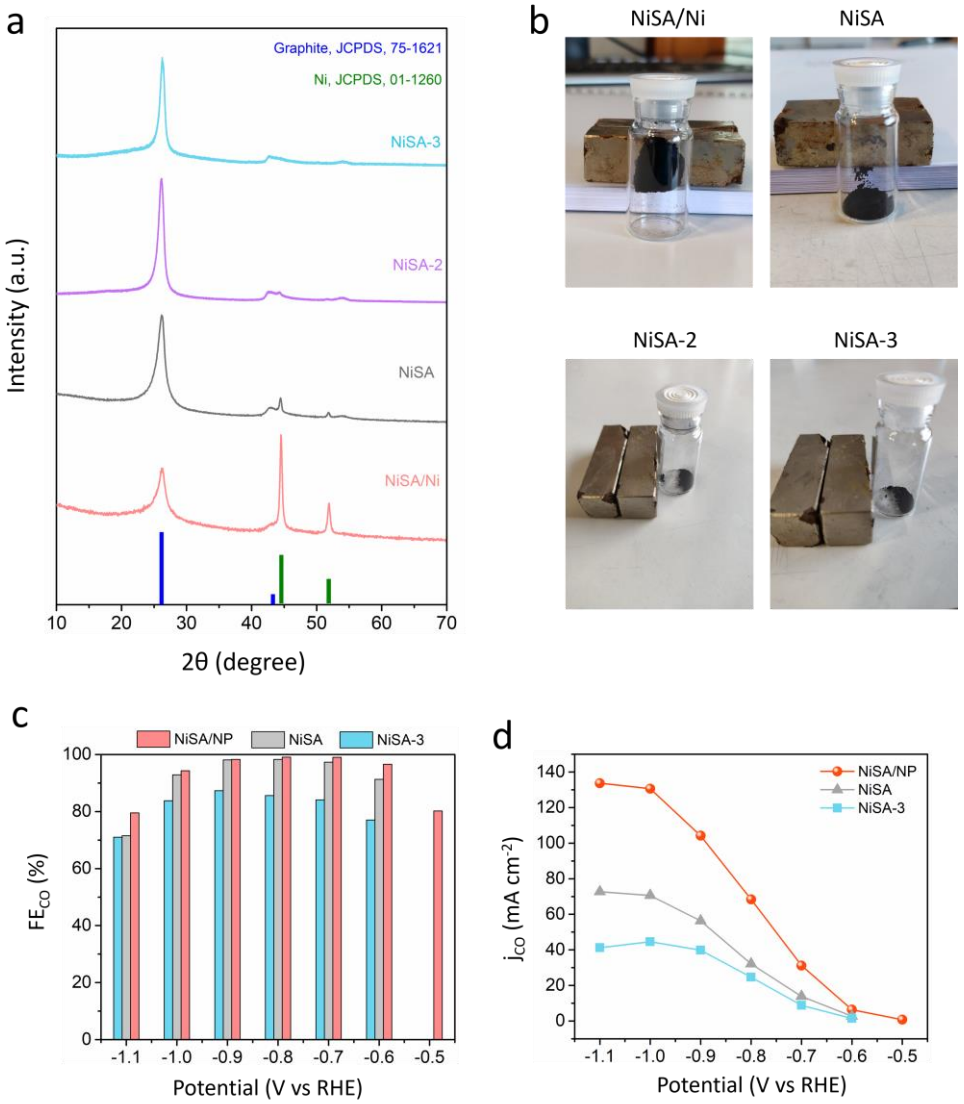

Supplementary Figure 8 | CO_2RR performance of pure NiSA. (a) XRD analysis. (b) Magnetic test. (c) FE_{CO} of catalysts. (d) j_{CO} of catalysts. The NiSA, NiSA-2, and NiSA-3 are treated by NH_4Cl for 1, 2, and 3 times respectively.

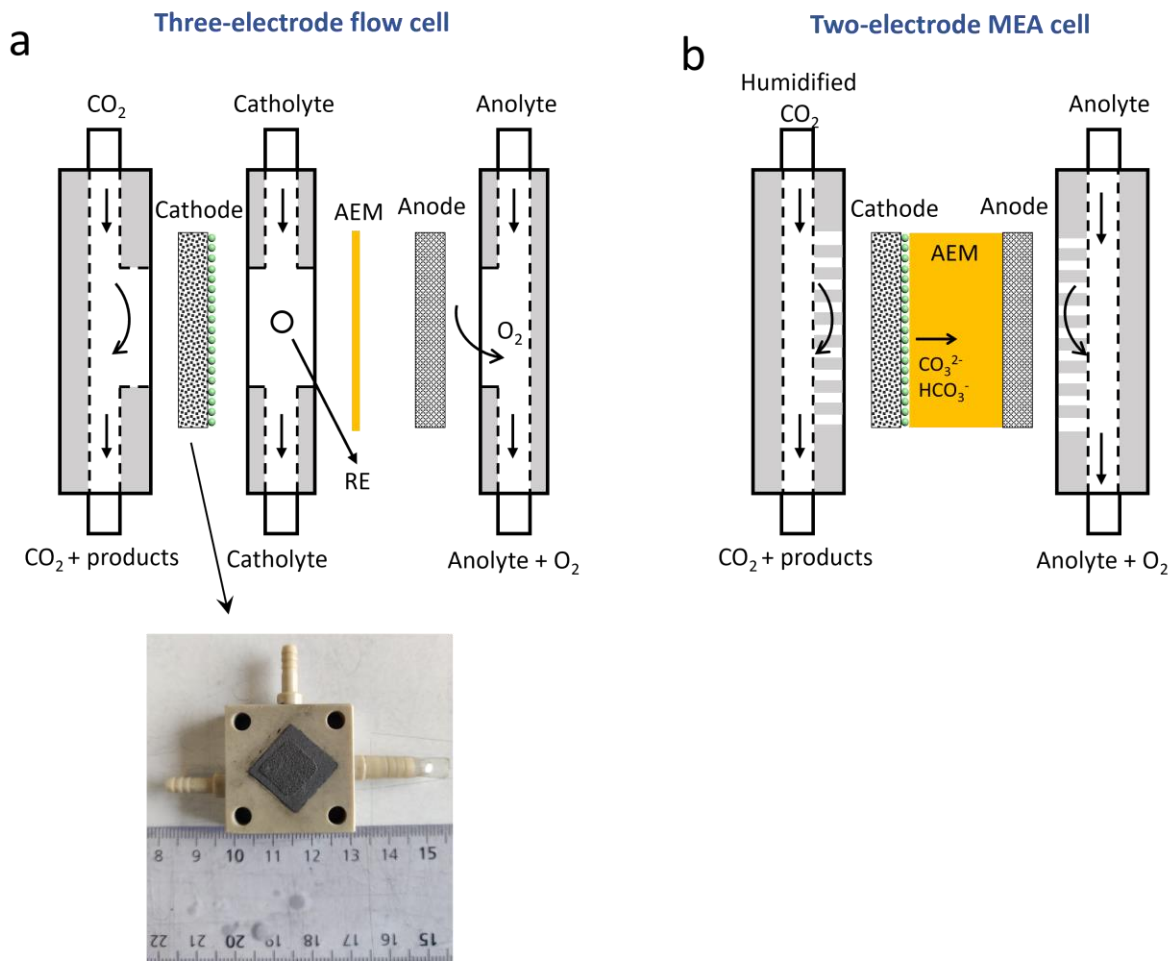

Supplementary Figure 9 | The schematic illustration of home-customized (a) three-electrode flow cell, and (b) two-electrode MEA device.

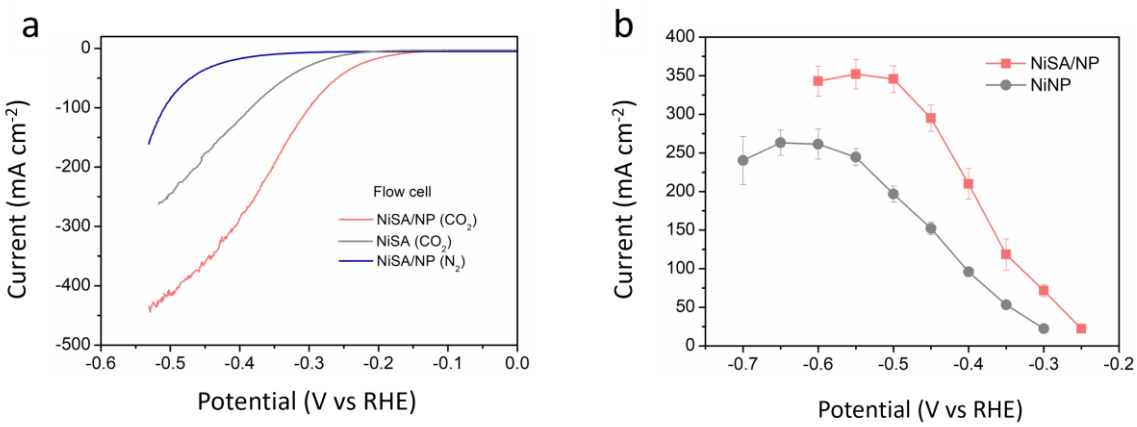

Supplementary Figure 10 | Electrochemical CO_2RR in flow cell with 1 M KOH electrolyte. (**a**) The LSV curve of NiSA/NP and NiSA at a scan rate of 10 mV s^{-1}. (**b**) j_{CO} of NiSA/NP and NiSA as a function of potential.

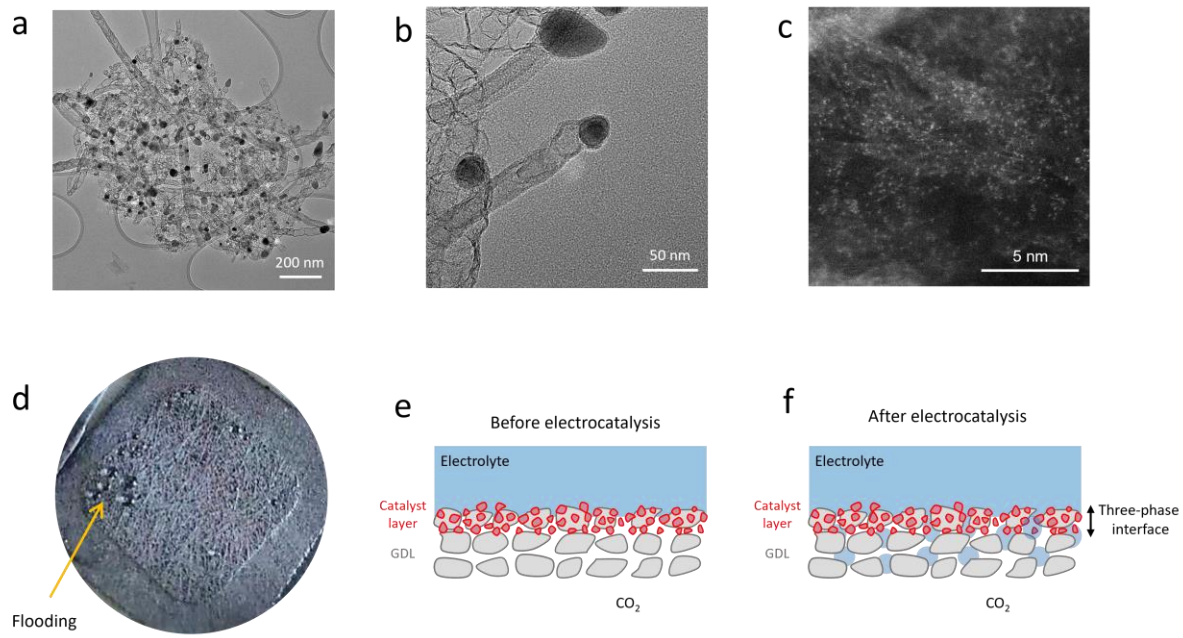

Supplementary Figure 11 | NiSA/NP after 10 h electrolysis at 100 mA cm^{-2}. (**a-c**) TEM and HADDF-STEM image of NiSA/NP. (**d**) The optical image of the gas diffusion electrode (backside) after testing. Schematic illustration of the three-phase interfaces among the catalyst, electrolyte, and CO_2 gas before (**e**), and after electrolysis (**f**), respectively.

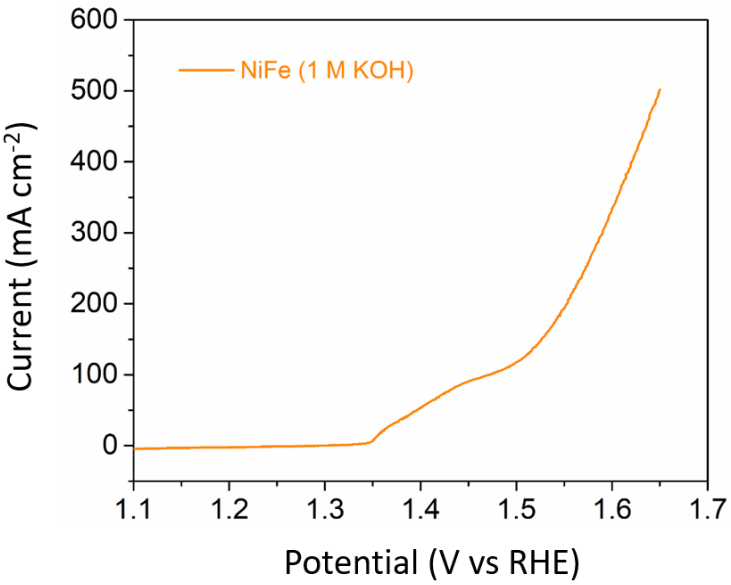

Supplementary Figure 12 | The LSV curve of NiFe OER catalyst in 1 M KOH.

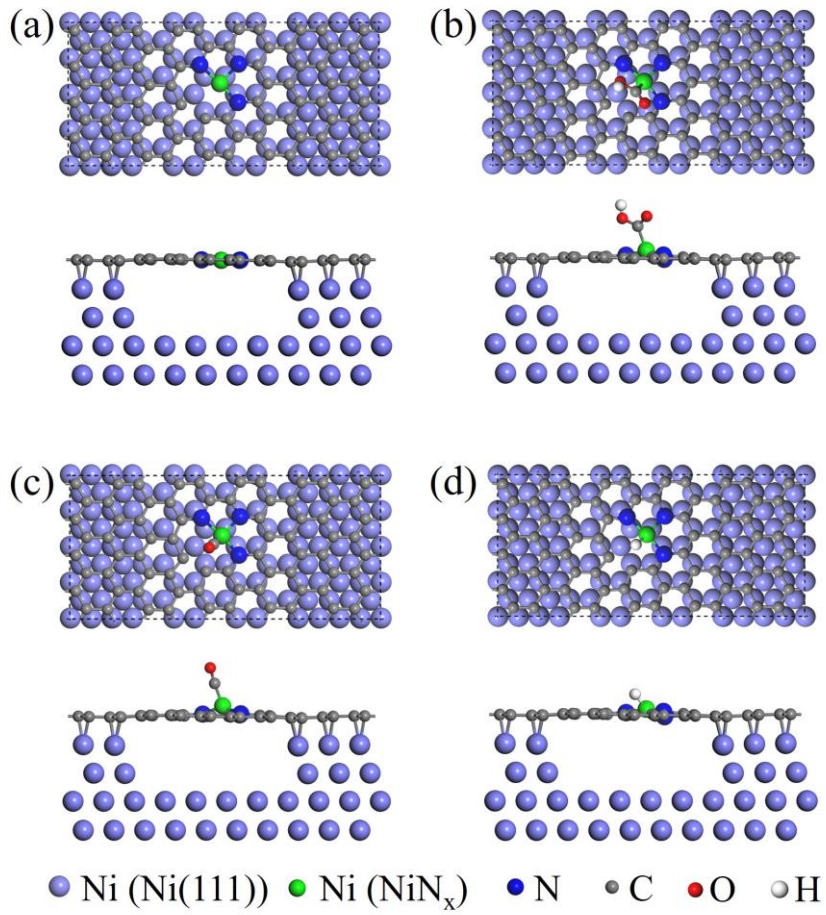

Supplementary Figure 13 | DFT Model 1 (NiN_3@Ni(111)). Top and side views of the (**a**) NiN_3@Ni(111) (**b**) NiN_3@Ni(111) with COOH*, (**c**) NiN_3@Ni(111) with CO*, and (**d**) NiN_3@Ni(111) with H*.

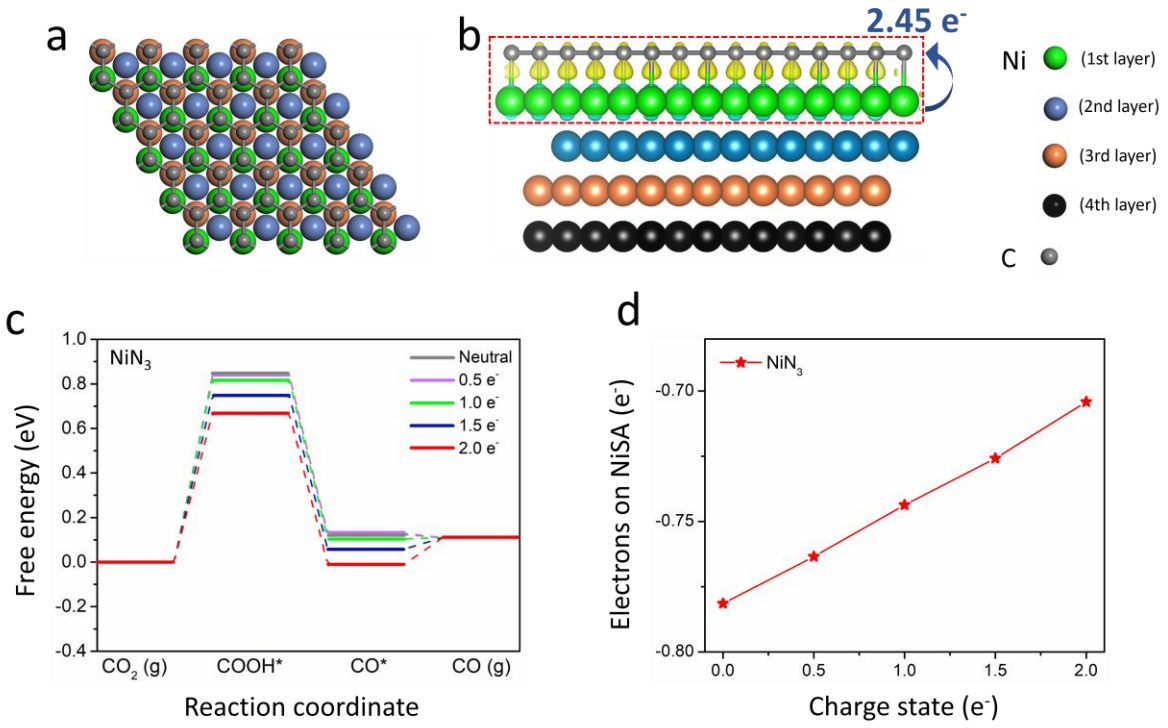

Supplementary Figure 14 | DFT Model 2 (Ni(111)/carbon). (**a**) Top view of the optimized structures of Ni(111)/carbon. (**b**) Side view of the deformation electronic density of the Ni(111)/carbon. (**c**) The calculated free energy diagrams for CO_2RR to CO on neutral and negatively charged NiN_3. (**d**) The number of electrons on Ni single atom in neutral and negatively charged NiN_3 structures.

Table S1. Inductively coupled plasma - optical emission spectrometry (ICP-OES) results on NiSA/NP and NiSA.

Sample	Ni wt%
NiSA/NP	8.8
NiSA	4.6

Table S2. Contribution to the free energy of adsorbates and non-adsorbed gas-phase molecules from ZPT correction, enthalpic temperature correction, and entropy contribution, respectively. All are given in eV.

Species	ZPE	$\int C_P dT$	*-TS*
$COOH^*$	0.62	0.10	-0.18
CO^*	0.19	0.08	-0.15
CO_2	0.31	0.10	-0.65
CO	0.14	0.09	-0.67
H_2	0.27	0.09	-0.42
H_2O	0.58	0.10	-0.65

Table S3. EXAFS fitting results of the Ni-N coordination shell.

Sample	Shell	N	R (Å)	σ^2 ($Å^2$)	ΔE_0 (eV)
NiSA	Ni-N	2.7	1.85	0.00478	-7.343

Table S4. Comparison of CO_2RR in H-cells with the recently reported Ni-N-C, Au, and Ag based catalysts.

Catalysis	FE_{CO} (%, V vs RHE)	Current density (mA cm^{-2}, V vs RHE)	Ref.
NiSA/NP	**99% at -0.8 V**	**131 mA cm^{-2} at -1.0 V**	**This work**
NiSA	**98% at -0.8 V**	**71 mA cm^{-2}at -1.0 V**	**This work**
NiSA/PCFM	96% at -0.7 V	56.1 mA cm^{-2} at -1.0 V	10
Ni(i)-NCNT@Ni_9Cu	97% at -0.73 V	32.9 mA cm^{-2} at -0.73 V	11
NC-CNTs (Ni)	90% at -0.8 V	~9 mA cm^{-2} at -1.0 V	12
A-Ni-NG	97% at -0.72V	22 mA cm^{-2} at -0.72 V	13
C-Zn_2Ni_1ZIF-8	98% at -0.83 V	72 mA cm^{-2} at -1.03 V	14
Ni-N_4/C-NH_2	96% at -0.7 V	~65 mA cm^{-2} at -1.0 V	15
Ag	~100% at -0.81 V	9 mA cm^{-2} at -1.0 V	16
AgNF	95% at -1.0 V	30 mA cm^{-2} at -1.2 V	17
Porous Ag	96% at -1.03 V	6 mA cm^{-2} at -1.0 V	18
Au-PA	62% at -0.8 V	10 mA cm^{-2} at -0.8 V	19
Nanoporous Au	98% at -0.5 V	12 mA cm^{-2} at -0.5 V	20
4H-Au	90% at -0.7 V	6 mA cm^{-2} at -0.7 V	21
$Au_{19}Cd_2$	95% at -0.7 V	45 mA cm^{-2} at -0.95 V	22

Table S5. Comparison of CO_2RR in MEA full cells with Ni-N-C, Au, Ag, CoPc catalysts.

Cathode	Anode	j_{CO}	Energy efficiency	FE_{CO}	Anode electrolyte	Temperature	Ref.
NiSA/NP	**NiFe**	**310 mA cm^{-2} at -2.3 V**	**57%**	**99%**	**1 M KOH**	**RT**	**This work**
Ni-N/PCFM	Ir/C	~300 mA cm^{-2} at -2.9 V	46%	99%	0.5 M $KHCO_3$	RT	23
Ag	IrO_x	~330 mA cm^{-2} at -3.0 V	38%	~85%	Water with 1 M CsOH activation	60 °C	24
Au	IrO_2	~300 mA cm^{-2} at -2.65 V	~43%	> 85%	Water	60 °C	25
CoPc	Ni foam	~175 mA cm^{-2} at -2.5 V	51%	~95%	1M KOH	RT	26

Reference

1 Kresse, G. & Hafner, J. Ab initio molecular-dynamics simulation of the liquid-metal–amorphous-semiconductor transition in germanium. *Phys. Rev. B* **49**, 14251 (1994).

2 Kresse, G. & Joubert, D. From ultrasoft pseudopotentials to the projector augmented-wave method. *Phys. Rev. B* **59**, 1758 (1999).

3 Kresse, G. & Furthmüller, J. Efficient iterative schemes for ab initio total-energy calculations using a plane-wave basis set. *Phys. Rev. B* **54**, 11169 (1996).

4 Perdew, J. P., Burke, K. & Ernzerhof, M. Generalized gradient approximation made simple. *Phys. Rev. Lett.* **77**, 3865 (1996).

5 Grimme, S., Antony, J., Ehrlich, S. & Krieg, H. A consistent and accurate ab initio parametrization of density functional dispersion correction (DFT-D) for the 94 elements H-Pu. *J. Chem. Phys.* **132**, 154104 (2010).

6 Tang, W., Sanville, E. & Henkelman, G. A grid-based Bader analysis algorithm without lattice bias. *J. Phys. Condens. Matter* **21**, 084204 (2009).

7 Peterson, A. A., Abild-Pedersen, F., Studt, F., Rossmeisl, J. & Nørskov, J. K. How copper catalyzes the electroreduction of carbon dioxide into hydrocarbon fuels. *Energy Environ. Sci.* **3**, 1311-1315 (2010).

8 Ju, W. *et al.* Understanding activity and selectivity of metal-nitrogen-doped carbon catalysts for electrochemical reduction of CO_2. *Nat. Commun.* **8**, 944, doi:10.1038/s41467-017-01035-z (2017).

9 Nørskov, J. K. *et al.* Trends in the exchange current for hydrogen evolution. *J. Electrochem. Soc.* **152**, J23-J26 (2005).

10 Yang, H. *et al.* Carbon dioxide electroreduction on single-atom nickel decorated carbon membranes with industry compatible current densities. *Nat. Commun.* **11**, 593 (2020).

11 Zhang, T. *et al.* Atomically Dispersed Nickel (I) on an Alloy-Encapsulated Nitrogen-Doped Carbon Nanotube Array for High-Performance Electrochemical CO_2 Reduction Reaction. *Angew. Chem.* **132**, 12153-12159 (2020).

12 Fan, Q. *et al.* Activation of Ni Particles into Single Ni–N Atoms for Efficient Electrochemical Reduction of CO_2. *Adv. Energy Mater.*, **10**, 1903068 (2019).

13 Yang, H. B. *et al.* Atomically dispersed Ni (i) as the active site for electrochemical CO 2 reduction. *Nat. Energy* **3**, 140 (2018).

14 Yan, C. *et al.* Coordinatively unsaturated nickel–nitrogen sites towards selective and high-rate CO_2 electroreduction. *Energy Environ. Sci.* **11**, 1204-1210 (2018).

15 Chen, Z. *et al.* Amination strategy to boost the CO_2 electroreduction current density of M–N/C single-atom catalysts to the industrial application level. *Energy Environ. Sci.* **14**, 2349-2356 (2021).

16 Wu, X. *et al.* Fast operando spectroscopy tracking in situ generation of rich defects in silver nanocrystals for highly selective electrochemical CO_2 reduction. *Nat. Commun.* **12**, 660 (2021).

17 Wei, L. *et al.* Thiocyanate-modified silver nanofoam for efficient CO_2 reduction to CO. *ACS Catal.* **10**, 1444-1453 (2019).

18 Abeyweera, S. C., Yu, J., Perdew, J. P., Yan, Q. & Sun, Y. Hierarchically 3D porous Ag nanostructures derived from silver benzenethiolate nanoboxes: enabling CO_2 reduction with a near-unity selectivity and mass-specific current density over 500 A/g. *Nano Lett.* **20**, 2806-2811 (2020).

19 Zhao, Y., Wang, C., Liu, Y., MacFarlane, D. R. & Wallace, G. G. Engineering surface amine modifiers of ultrasmall gold nanoparticles supported on reduced graphene oxide for improved electrochemical CO_2 reduction. *Adv. Energy Mater.* **8**, 1801400 (2018).

20 Lu, X., Yu, T., Wang, H., Qian, L. & Lei, P. Electrochemical Fabrication and Reactivation of Nanoporous Gold with Abundant Surface Steps for CO_2 Reduction. *ACS Catal.* **10**, 8860-8869 (2020).
21 Wang, Y. *et al.* Undercoordinated Active Sites on 4H Gold Nanostructures for CO_2 Reduction. *Nano Lett.* **20**, 8074-8080 (2020).
22 Li, S. *et al.* Boosting CO_2 electrochemical reduction with atomically precise surface modification on gold nanoclusters. *Angew. Chem.* **133**, 6421-6426 (2021).
23 Jeong, H.-Y. *et al.* Achieving highly efficient CO_2 to CO electroreduction exceeding 300 mA cm− 2 with single-atom nickel electrocatalysts. *J. Mater. Chem. A* **7**, 10651-10661 (2019).
24 Endrődi, B. *et al.* Operando cathode activation with alkali metal cations for high current density operation of water-fed zero-gap carbon dioxide electrolysers. *Nat. Energy* **6**, 439-448 (2021).
25 Yin, Z. *et al.* An alkaline polymer electrolyte CO_2 electrolyzer operated with pure water. *Energy Environ. Sci.* **12**, 2455-2462 (2019).
26 Ren, S. *et al.* Molecular electrocatalysts can mediate fast, selective CO_2 reduction in a flow cell. *Science* **365**, 367-369 (2019).